Exploring the Energy Landscape of Nucleic Acid Hairpins Using Laser Temperature-Jump and Microfluidic Mixing

Ranjani Narayanan,[†,‡,±] Li Zhu,[¶,⊥,±] Yogambigai Velmurugu,[†] Jorjethe Roca,[†] Serguei V. Kuznetsov,[†] Gerd Prehna,[&] Lisa J. Lapidus,*[,¶] and Anjum Ansari*[,†,§]
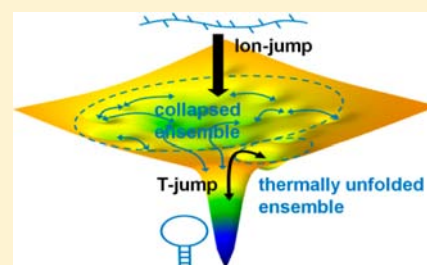
Departments of [†]Physics and [§]Bioengineering, and [&]Center for Structural Biology, University of Illinois at Chicago, Chicago, Illinois 60607, United States

[¶]Department of Physics and Astronomy, Michigan State University, East Lansing, Michigan 48824, United States

[⊥]Advanced Photonics Center, Southeast University, Nanjing 210096, China

Ⓢ *Supporting Information*

ABSTRACT: We have investigated the multidimensionality of the free energy landscape accessible to a nucleic acid hairpin by measuring the relaxation kinetics in response to two very different perturbations of the folding/unfolding equilibrium, either a laser temperature-jump or ion-jump (from rapid mixing with counterions). The two sets of measurements carried out on DNA hairpins (4 or 5 base pairs in the stem and 21-nucleotide polythymine loop), using FRET between end labels or fluorescence of 2-aminopurine in the stem as conformational probes, yield distinctly different relaxation kinetics in the temperature range 10−30 °C and salt range 100− 500 mM NaCl, with rapid mixing exhibiting slower relaxation kinetics after an initial collapse of the chain within 8 μs of the counterion mixing time. The discrepancy in the relaxation times increases with increasing temperatures, with rapid mixing times nearly 10-fold slower than T-jump times at 30 °C. These results rule out a simple two-state scenario with the folded and unfolded ensemble separated by a significant free energy barrier, even at temperatures close to the thermal melting temperature T_m. Instead, our results point to the scenario in which the conformational ensemble accessed after counterion condensation and collapse of the chain is distinctly different from the unfolded ensemble accessed with T-jump perturbation. Our data suggest that, even at temperatures in the vicinity of T_m or higher, the relaxation kinetics obtained from the ion-jump measurements are dominated by the escape from the collapsed state accessed after counterion condensation.

INTRODUCTION

Hairpins or stem-loop structures are the simplest secondary structural motifs in nucleic acids, and they play important roles in regulating transcription in vivo,[1−3] as intermediates in genetic recombination,[4,5] as target sites for protein recognition,[6] and as nucleation sites for initiating RNA folding.[7] Their biological functions depend on their stability and dynamics. The simplicity of their structures also makes them ideal testing grounds for novel computational studies,[8−16] allowing direct comparisons with experiments.

The thermodynamics and folding kinetics of single-stranded (ss) DNA and RNA hairpins have been of interest to biophysical scientists since at least the early seventies.[17] The earliest measurements of the relaxation dynamics of nucleic acids in response to capacitor discharge temperature-jump (T-jump) revealed single-exponential kinetics,[18−20] suggesting an all-or-none folding/unfolding behavior, with distinct "valleys" in the free energy landscape corresponding to the "folded" and "unfolded" ensemble, separated by a significant free energy barrier. In the past decade or so, new and improved techniques have started to reveal the underlying ruggedness in the energy landscape of even these simple structures, and have led to a renewed discussion on whether nucleic acid hairpins fold in a

cooperative (two-state) manner or have metastable partially folded or misfolded intermediates in the folding pathway.

To some extent this debate stems from the ability of different experimental tools with enhanced sensitivities and significant improvement in time-resolution to examine the fine structure in each of the "valleys". A significant breakthrough in the ability of experimentalists to investigate the dynamics on different time scales with exquisite sensitivity has come from laser T-jump techniques that have pushed the time-resolution from microseconds to nanoseconds[21−23] and even picoseconds,[24] together with the ability to measure the relaxation kinetics with multiple probes that include UV[21,25,26] and infrared[22] absorbance, fluorescence of nucleotide analogs,[23,27] and extrinsically attached fluorescent dyes.[24,26] These measurements have started to reveal deviations from a two-state behavior. An early example of this is T-jump measurements carried out by Porschke on duplex RNA at temperatures below the melting temperature for the helix-to-coil transition,[28] where he observed a rapid phase, with characteristic relaxation time of ~200 ns, and assigned it to the unzipping or "fraying" at the

ends. A much slower phase, occurring on time scales of milliseconds or longer at temperatures near T_m, was the overall association/dissociation of the duplex strands.[29] Deviations from a two-state behavior were also evident in thermodynamic measurements that showed nonoverlapping sigmoidal transitions of DNA hairpin melting when measured by fluorescence of incorporated fluorescent analogs and UV absorbance measurements on the same hairpins, with the fluorescence melting temperature shifted to lower temperatures, indicative of a "pre-melting" transition.[30] A rapid kinetics phase corresponding to stem fraying dynamics has now been observed in T-jump studies on RNA hairpins.[21,23,31] Other measurements show evidence for dynamics in the "unfolded" ensemble that includes stacking/unstacking of the bases, as well as the potential for mis-stacked pairs.[22−24,31] Thus, these additional kinetic phases primarily reflect rapid dynamics in the folded or unfolded ensemble of the two-state approximation, and not necessarily stable intermediate states.

Perhaps the biggest challenge to the notion of cooperative folding behavior comes from fluctuation correlation spectroscopy measurements of Van Orden and co-workers on ssDNA hairpins with large (21-nt long poly(dT)) loops.[32] These studies pointed to a three-state folding mechanism, with evidence, albeit indirect, for a stable, long-lived intermediate state from which folding to the native hairpin conformation occurs on very slow time scales, longer than the few milliseconds time window of FCS measurements. These studies represented a departure from earlier FCS measurements, by Libchaber and co-workers, also on ssDNA hairpins with 8- to 30-nt long poly(dT) or poly(dA) loops, that reported two-state folding/unfolding behavior,[33,34] and another FCS study, on ssDNA hairpins with 30-nt long poly(dA) loops, by Klenerman and co-workers, that showed stretched exponential kinetics on the FCS time scale.[35] Some of the discrepancies between these different FCS measurements on hairpins, all with very similar stem compositions, may be attributed to the difficulties in separating the contribution to the measured fluorescence fluctuations as a result of diffusion of molecules in the confocal volume from conformational dynamics of interest, which, as demonstrated by the Levitus group, could introduce distortions in the observed correlation functions.[36] By designing small hairpins that fold on time scales faster than the molecular diffusion time (2-bp stem and 4−5 nt loop), the Sauer group provided a clear demonstration of stretched exponential kinetics in their FCS measurements.[37] However, for hairpins with large loops, whose folding times overlap with their molecular diffusion times, the inconsistencies in FCS measurements from different groups leave a lingering question as to whether there are indeed long-lived collapsed states in the folding pathway.

In this study we explore these questions by employing two distinct experimental approaches: laser temperature-jump and ion-jump induced by rapid (microfluidic) mixing. The motivation for this study stems from the intrinsic limitations in exploring the energy landscape using one single technique, which may give only a restricted view, especially if there are traps whose population in a kinetics measurement depends on the initial state of the system. In a temperature-jump experiment, the initial population, immediately after the T-jump, is characteristic of the equilibrium population at the initial temperature and, for small T-jumps, the system may not have enough time to populate traps that require long (or uphill) excursions in the unfolded region of the energy

landscape. In contrast, in a mixing experiment, the initial condition (in our case a negligible concentration of counterions) results in an initial population of highly extended chain molecules, with folding initiated by rapidly switching to higher ionic strength conditions in the mixing device. The relaxation rates measured in response to the two very different perturbation techniques are expected to be identical if the energy landscape is indeed dominated by two distinct valleys, and the collapsed state accessed rapidly after ion-jump samples the same conformational region as the thermally unfolded ensemble. If, on the other hand, there are stable (or metastable) on- or off-pathway, intermediates, then one might expect more than one relaxation phase, with the amplitudes in different phases highly dependent on the initial populations. A third scenario could well be that folding behavior of nucleic acid hairpins is dominated by a diffusive search on a relatively flat energy landscape, with different regions of the energy landscape accessed by ion-jump versus T-jump.

This study focuses on two ssDNA hairpins. The first is a 4-bp stem hairpin with a loop of 21 thymine residues (T_{21}) whose sequence was chosen to be identical to the one used in a study by the Van Orden group, and for which they could resolve two distinct relaxations within their FCS time window.[38] The second is a slightly longer (5-bp stem, T_{21} loop) hairpin with similar sequence composition as the hairpins at the center of the controversy as to whether their kinetics are single-exponential,[33,34] stretched exponential,[35] or incomplete[32] on the FCS time scale. Our measurements on both hairpins reveal qualitatively similar behavior, with predominantly single-exponential kinetics observed in both T-jump and rapid mixing studies, especially at high (>100 mM NaCl) salt, and no strong evidence for missing relaxation phases on longer than millisecond time scale, although we cannot rule out missing amplitudes on short (<1−10 μs) time scales. In particular, fast polymeric collapse is observed within the 8 μs mixing time of the rapid mixing device.

The most notable result from this study is that the relaxation times that characterize the folding/unfolding kinetics measured in response to the two distinct perturbations, T-jump and ion-jump (in rapid mixing), are found to be different for identical final temperature and ionic strength conditions, with the rapid mixing relaxation times as much as 10-fold slower in comparison with T-jump relaxation times, at temperatures approaching ~30 °C. Therefore, although the observed single-exponential relaxation kinetics may suggest an apparent two-state behavior, the distinct relaxation times obtained from the two sets of measurements indicate that the unfolded ensemble accessed in T-jump is distinctly different from the unfolded ensemble accessed after rapid addition of counterions and the initial collapse.

■ EXPERIMENTAL SECTION

DNA Samples. Experiments were conducted on two DNA sequences with a 21-thymine loop: a 4-bp stem hairpin 5′-AACC(T_{21})GGTT-3′ (denoted as VS4T21) labeled with FAM at its 5′ end and ALEXA647 at its 3′ end, and a 5-bp stem hairpin 5′-CCCXA(T_{21})TTGGG-3′ (denoted as LS5T21), where X denotes the fluorescent analogue 2-aminopurine (2AP) substituted instead of adenine in the stem region. The FRET-labeled and unlabeled oligomers were obtained from Integrated DNA Technologies Inc. (Coralville, IA), while the 2AP-labeled hairpins were obtained from Oligos Etc. (Wilsonville, OR). All hairpins were purchased with HPLC purification. Buffer conditions were 2.5 mM TRIS-HCl, pH 8.0, 250 μM EDTA, for all measurements on the FRET-labeled VS4T21

Table 1. Thermodynamic Parameters for DNA Hairpin Melting[a]

	VS4T21	VS4T21	VS4T21	LS5T21	LS5T21	LS5T21
[NaCl]	100 mM	250 mM	500 mM	100 mM	200 mM	500 mM
T_m (°C)	8.6 ± 2.3 (5.2 ± 2.4)	19.5 ± 0.7 (14.7 ± 2.8) 18.4 ± 1.2[b] 16.5 ± 0.5[d]	26.8 ± 0.9 (22.8 ± 0.1)	15.4 ± 3.3	22.9 ± 1.4 27.4 ± 1.4[c] 26.0 ± 1.0[d]	27.3 ± 1.5
ΔH_{vH} (kcal/mol)	−30.2 ± 1.1 (−37.2 ± 6.9)	−32.1 ± 1.3 (−34.7 ± 6.2) −24.1 ± 1.9[b] −11.4 ± 0.6[d]	−30.4 ± 2.5 (−33.3 ± 0.2)	−40.9 ± 14.8	−32.2 ± 4.9 −32.3 ± 2.9[c] −24.7 ± 1.4[d]	−30.5 ± 5.3

[a]From fluorescence measurements; numbers in parentheses are from analysis of acceptor ratio data. [b]From UV absorbance measurements on unlabeled hairpins, with strand concentrations in the range: 3.7−81.3 μM. [c]From UV absorbance measurements on unlabeled hairpins, with strand concentrations in the range: 3.0−61.9 μM. [d]From DSC measurements on unlabeled hairpins, as described in the Supporting Information.

hairpins, with NaCl concentrations of 0, 100, 250, or 500 mM, and 5 mM sodium cacodylate buffer, pH 7.0, 50 μM EDTA, for all measurements on the 2AP-labeled LS5T21 hairpins, with NaCl concentrations of 0, 100, 200, or 500 mM.

Equilibrium Measurements. Fluorescence measurements were obtained with a Fluoromax-2 spectrofluorimeter (Horiba Jobin Yvon Instruments, Edison, NJ) equipped with a temperature-controlled circulating bath. FRET-labeled hairpins were excited at 495 nm (absorption maximum of FAM), or at 650 nm (to directly excite the acceptor ALEXA647), and the emission spectra were collected over the wavelength range 500−700 nm and temperature range 5−60 °C. 2AP-labeled hairpins were excited at 314 nm and emission spectra were collected over the wavelength range 330−450 nm, and temperature range 5−50 °C. The fluorescence melting profiles were obtained from the measured intensity at 520 nm (maximum of FAM fluorescence) for FRET-labeled hairpins, and from measured intensity at 368 nm (maximum of 2AP fluorescence) for 2AP-labeled hairpins.

An independent estimate of the thermodynamics of FRET-labeled hairpins was obtained from measurements of the acceptor ratio r_A, which was calculated as follows.[39] The donor fluorophore was excited at 495 nm, and the emission spectra were collected from 500 to 700 nm. A normalized emission spectrum of a donor-only labeled sample, excited at 495 nm, was subtracted from the emission spectrum to isolate the acceptor emission. The acceptor fluorophore was directly excited at 650 nm and emission spectra collected in the same wavelength range as before. The area under the corrected spectrum (after subtraction of donor fluorescence), integrated from 658 to 678 nm, was divided by the area under the directly excited emission spectrum, also integrated from 658 to 678 nm, to obtain the value of the acceptor ratio r_A.

The melting profiles obtained from fluorescence intensity measurements $F(T)$ or acceptor ratio measurement $r_A(T)$ were then fit to a two-state van't Hoff transition with linear upper and lower baselines, as described in Narayanan et al.[26] The two baselines were constrained to have the same slope. The thermodynamic fitting parameters thus obtained are ΔH_{vH}, the enthalpy of the fully folded hairpin relative to the unfolded state, and T_m, the melting temperature, for each sample and solvent conditions. The primary source of error in the fitting parameters is from incomplete information about the temperature dependence of the upper and lower baselines. The uncertainties reported in Table 1 were determined by estimating the deviations in the thermodynamic parameters when the baselines were allowed to have independently varying slopes.

Laser T-Jump Spectrometer. The T-jump spectrometer consists of a multimode Q-switched Nd:YAG laser (Continuum Surelite I(II), fwhm = 6 ns, 400(600) mJ/pulse at 1.06 μm) that is used to pump a 1 m long Raman cell consisting of high-pressure methane gas. The energy of the 1.54 μm beam, measured at the sample position, was adjusted to be ∼40 mJ/pulse. The 1.54 μm beam was focused to ∼1 mm (fwhm) on the sample cell and achieved a typical T-jump of about 5−10 °C in 0.5 mm path length cell. The probe source was either a 488 nm, 20 mW diode laser (Newport PC13589), to excite FAM, or a 284 nm, 10 mW frequency-doubled Krypton laser (Lexel 95-SHG-284-QS), to excite 2AP. The fluorescence intensities were filtered by band-pass filters (Semrock FF536-40-25 for FAM fluorescence, with

>95% transmission in the wavelength range 515−555 nm, and Semrock FF370-36-25 for 2AP fluorescence, with >90% transmission in the wavelength range 352−388 nm) and measured with a Hamamatsu R928 photomultiplier (PMT) tube coupled to a 300 MHz preamplifier (SR445A, Stanford Research) and a 500 MHz transient digitizer (Hewlett-Packard 54825A). Sample temperature was controlled by a circulating bath (Neslab RTE110) and measured by a thermistor YSI 44008 in contact with the sample holder. Sample fluorescence at each temperature was collected on two different time scales, spanning 500 μs and 2.5 ms, with 25000 data points in each trace. Kinetics traces acquired on the different time scales were then matched together prior to further analysis.

Rapid Mixing Apparatus. Folding experiments were conducted through a microfluidic ultrarapid mixer of the type developed by Knight et al.[40] and Hertzog et al.[41,42] and modified by Yao et al.[43] and Waldauer et al.[44] The mixer is made from a 500 μm thick fused silica wafer with channels typically etched 10 μm deep and a second 170 μm wafer bonded on top to seal the device. All flows are in the laminar regime and streamlines can be calculated by mathematical simulations (COMSOL Multiphysics, Stockholm Sweden). Flow rates are controlled by pressure transducers that apply a pressure to the reservoirs of a temperature-controlled manifold. Time is calculated from measured positions in the chip and the calculated flow rate at that position.

Fluorescence changes can be observed at various times beyond mixing by using a custom-built confocal instrument. For 2AP measurements a frequency-doubled Argon-Ion laser (258 nm) is focused by an infinity-corrected UV objective (OFR 40x-266) to ∼1 μm spot in the mixer. Fluorescence is collected by the same objective by using a dichroic mirror (Chroma 300 dclp) and a filter (UG1), focused on a 100 μm pinhole to remove excitation light, and detected with a photon counter (Hamamatsu H7421-40). The chip position is controlled by two translation stages, a mechanical screw driven stage (KL-Series 12-6436, SEPREX Corp, Campbell CA) for coarse (∼100 μm) steps and a piezoelectric nanopositioner (Mad City Laboratories Nano-LP100, Madison WI) for submicrometer steps. For FRET measurements, the excitation wavelength is 488 nm (Melles Griot Ion Laser) focused by a visible high NA objective (Olympus UPLSAPO 60XW 1.2 NA) to a spot size ∼0.25 μm by using a 500 nm dichroic mirror (500 DCXT, Omega Optical, Brattleboro, VT). Only the donor emission is detected with the photon counter for purposes of locating the mixing region on the chip. After this initial measurement, a flip-up mirror then directs the emission onto the narrow entrance slit of a spectrograph (MicroHR, Horiba Instruments Inc., Irvine CA) and spread onto a 1024 × 225 pixel CCD array (iDus 420A-BU, Andor Technology, South Windsor, CT). This allows simultaneous detection of fluorescence spectra between ∼510 and ∼810 nm. Certain channels of the CCD were designated Donor and Acceptor and the sum of these intensities, I_D and I_A, respectively, was used to calculate the proximity ratio as $I_A/(I_D + I_A)$.

During a mixing experiment, the DNA in initial conditions (0 M NaCl) proceeds down a channel and is met on either side by a flow with higher salt concentration flowing ∼100 times faster, causing the center stream to constrict to a jet ∼100 nm wide. Figure S1 (Supporting Information) shows a typical image of the mixing region.

18954

dx.doi.org/10.1021/ja301218e | *J. Am. Chem. Soc.* 2012, 134, 18952−18963

Mixing of the salt is due to rapid diffusion into this jet. Because the jet is smaller than the diffraction limit of the objective, the instrument response is an enormous loss of fluorescence intensity during mixing. This response can be eliminated when measuring 2AP emission by making a control experiment in which the salt condition is unchanged after mixing and making a ratio point-by-point of these two measurements along the exit channel. Since proximity ratio on FRET-labeled samples is obtained from a ratio of two intensities from the same measurement, this procedure is unnecessary. The relaxation traces obtained on the FRET-labeled samples in the rapid mixing apparatus were analyzed by using both proximity ratio and donor intensity as probes, since the latter probe provides a direct comparison with measurements made on the T-jump apparatus.

Within the first few micrometers of the exit channel, the flow rate of the DNA increases ∼100-fold and the time after mixing must be calculated from the COMSOL simulations. Figure 7d shows the exact times which were used to determine the mixing time. Beyond the mixing region in the straight observation channel, the linear flow rate is constant and can be determined from the applied pressures and a simple resistance model. Only data in the constant flow region are used in fitting. The calculated flow rate has been confirmed by microparticle image velocimetry within 95% of the calculated flow rates.[41] The largest source of error in determining the time at a particular location is the spatial resolution (∼1 μm) of the confocal microscope.

Analysis of Relaxation Kinetics. The kinetics traces acquired with T-jump or rapid mixing measurements were analyzed either as a single- or double-exponential decay, or by maximum entropy analysis as described in the Supporting Information. All T-jump relaxation kinetics were well described as a single-exponential decay, and the relaxation times thus obtained, together with the equilibrium constants obtained from a two-state fit to the melting profiles, were used to calculate the hairpin folding (τ_F) and unfolding (τ_U) times at each temperature.

■ RESULTS

We have carried out laser temperature-jump and ion-jump in rapid mixing measurements on two hairpins, referred to as VS4T21 and LS5T21, which consist of either 4 or 5 base pairs in the stem and a 21-thymine loop. We use either FRET measurements on end-labeled hairpins (as in VS4T21) or 2AP fluorescence measurements with 2AP substitution in the stem (as in LS5T21) to obtain the thermodynamics and kinetics of folding/unfolding.

Equilibrium Fluorescence Measurements on FRET-Labeled VS4T21 Hairpin. Fluorescence emission spectra of VS4T21 labeled with FAM and ALEXA647, obtained at different temperatures for samples in 0, 100, 250, and 500 mM NaCl, are shown in Figure S2 (Supporting Information). The emission spectra, with excitation at 495 nm, show a dominant peak from the donor label FAM, centered at 520 nm, and a much weaker peak from the acceptor label, centered at 668 nm. As the temperature is increased, the donor emission intensity first increases as the hairpin melts, and then, at temperatures well above the melting transition where the hairpin is completely unfolded, the donor fluorescence starts to decrease with increasing temperature, reflecting the decrease in the quantum yield of the donor with increasing temperature. This behavior is clearly apparent in a plot of the maximum of the fluorescence emission spectra, at 520 nm, as a function of temperature (Figure 1a). Measurements on hairpins labeled with only donor and no acceptor also show a slight increase in fluorescence emission intensity as the hairpin melts (data not shown), which we attribute to some interaction of the label with the hairpin stem. However, the predominant contribution to the increase in donor intensity of the double-labeled hairpins
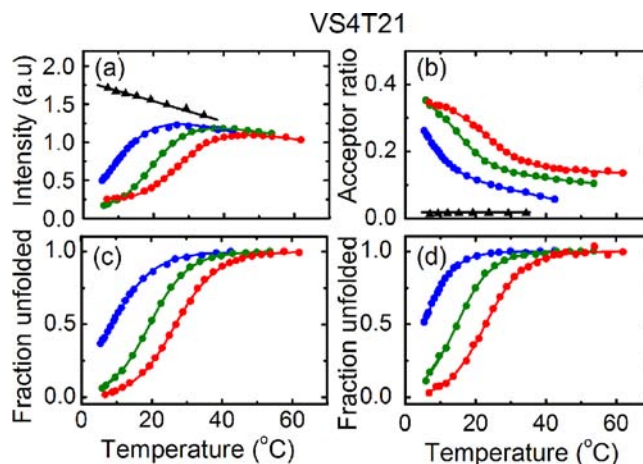

Figure 1. Equilibrium melting profiles of VS4T21 hairpins. (a) The fluorescence emission intensity of FRET-labeled DNA hairpin VS4T21, measured at 520 nm after excitation at 495 nm, is plotted as a function of temperature in 0 M NaCl (black triangles), 100 mM NaCl (blue circles), 250 mM NaCl (green circles), and 500 mM NaCl (red circles). (b) The acceptor ratio (r_A) obtained as defined in the text is plotted as a function of temperature. (c, d) The fraction unfolded, obtained from a two-state analysis of the fluorescence emission intensity data shown in panel a, and the acceptor ratio data shown in panel b, respectively, are plotted as a function of temperature for the three different salt concentrations. The symbols in panels b−d are as described for panel a. All measurements were made with ∼1 μM strand concentration in 2.5 mM Tris-HCl pH 8.0, 250 μM EDTA, and varying NaCl concentrations.

during the melting transition arises from an increase in the donor−acceptor distance as the hairpin unfolds. This result is also evident from the temperature dependence of the change in the acceptor ratio (r_A) (Figure 1b), as defined in the Experimental Section, which reflects directly the change in FRET efficiency and hence the end-to-end distance as the hairpin unfolds. An important result from this analysis is that the acceptor ratio at 0 M NaCl has a value $r_A \approx 0$, indicating little or no energy transfer between the FRET labels at the ends. In contrast, in the presence of monovalent ions, the acceptor ratio for the thermally unfolded ensemble at high temperatures ranges from $r_A \approx 0.05$ in 100 mM NaCl to $r_A \approx 0.13$ in 500 mM NaCl. Thus, in the absence of any counterions, the polynucleotide chain appears to adopt an extended conformation, as might be expected for a stiffer polymer.

The melting profiles, obtained from either the maximum intensity of the donor emission spectra (at 520 nm) or the acceptor ratio (r_A), measured on the double-labeled samples, clearly show melting transitions in the presence of monovalent ions, but no transition in the absence of salt, indicating an undetectable fraction of folded hairpins at 0 M NaCl. A fit to the melting profiles using a two-state folding/unfolding transition yields the fraction of unfolded molecules as a function of temperature (Figure 1c,d). The thermodynamic parameters for hairpin melting, from donor intensity (acceptor ratio) measurements, are summarized in Table 1, and yield melting temperatures of 9 (5) °C, 20 (15) °C, and 27 (23) °C, respectively, at 100, 250, and 500 mM NaCl, respectively. The values of T_m are less well determined at the lower salt concentrations, where the complete transition is not observed in the temperature window of our measurements.

Previous thermodynamics measurements on this hairpin, carried out by the Van Orden group, were done with

18955

dx.doi.org/10.1021/ja301218e | *J. Am. Chem. Soc.* 2012, 134, 18952−18963

rhodamine- and dabcyl-labeled hairpins, where dabcyl served as a quencher of rhodamine fluorescence. These measurements yielded $T_m \approx 27$ °C in 100 mM NaCl, significantly higher than the ~9 °C that we obtain with donor intensity measurements under identical buffer conditions. Since the only difference between the two studies appears to be the choice of attached labels, we also measured the melting profiles for unlabeled hairpins using UV absorbance as a probe. For the unlabeled (control) measurements, we chose 250 mM NaCl as our salt condition, in order to ensure that the hairpin is predominantly folded at low temperatures. Furthermore, we carried out UV absorbance measurements at several different strand concentrations, to examine any contribution to the thermodynamics from duplex formation. The absorbance measurements, shown in Figure S3 (Supporting Information) yield T_m values within 3 °C for strand concentrations ranging from 3.7 to 81.3 μM, with an average value of 18.4 ± 1.2 °C, in good agreement with the values of 15−20 °C that we obtained from the fluorescence measurements on our FRET-labeled samples. Thus, neither the concentration of the samples nor the choice of our labels had any significant effect on the thermodynamic stability of these hairpins. As an independent control, we also performed differential scanning calorimetry (DSC) measurements on these hairpins, as described in the Supporting Information, with consistent values for $T_m = 16.5 \pm 0.5$ °C (Figure S6a, Supporting Information).

Equilibrium Fluorescence Measurements on 2AP-Labeled LS5T21 Hairpin. The fluorescence emission spectra measured on 2AP-labeled LS5T21 at four different salt concentrations (0, 100, 200, and 500 mM NaCl) are shown in Figure S4 (Supporting Information) and the melting profiles, obtained from the maximum of the 2AP fluorescence emission (at 368 nm), are shown in Figure 2. The 2AP fluorescence is sensitive to the extent of stacking of the nucleotide analogue with its neighbors, and is found to increase when the stem melts. In contrast, measurements in 0 M NaCl show only a monotonic decrease in fluorescence intensity due to the decrease in 2AP quantum yield with increasing temperature. Thermodynamic parameters obtained from a two-state fit to the 2AP fluorescence melting profiles are summarized in Table 1, and yield melting temperatures of 15, 23, and 27 °C, respectively, at the three salt concentrations. To determine the effect of 2AP substitution on the stability of the hairpins, we also measured UV absorbance melting profiles on unlabeled hairpins. These measurements, shown in Figure S5 (Supporting Information), yield $T_m = 27.4 \pm 1.4$ °C in 200 mM NaCl, for strand concentrations ranging from 3.0 to 61.9 μM. Calorimetry measurements on this hairpin yielded $T_m = 26.0 \pm 1.0$ °C (Figure S6b, Supporting Information). Thus, measurements on unlabeled hairpins are about 3−5 °C higher than the 2AP-labeled samples under identical buffer conditions, which is within the range of previously reported effects of thermodynamic destabilization of duplex regions upon 2AP insertion.[30]

Previous measurements on similar 5-bp stem hairpins, in the Libchaber and Van Orden groups, with rhodamine/dabcyl labels, again showed much more stable hairpins than what we find. Bonnet et al.[33] measured $T_m \approx 38$ °C in 100 mM NaCl, and Goddard et al.[34] measured $T_m \approx 48$ °C in 250 mM NaCl, on hairpins with a sequence identical to that of LS5T21, while Jung et al.[32] measured $T_m \approx 43$ °C in 100 mM NaCl for a hairpin of identical length and composition, but slightly altered sequence: 5′-AACCC(T_{21})GGGTT-3′. We used the same
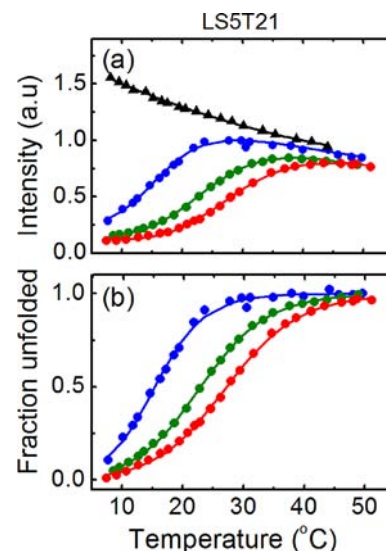

Figure 2. Equilibrium melting profiles of LS5T21 hairpins. (a) The fluorescence emission intensity of 2AP-labeled LS5T21 hairpin, measured at 368 nm after excitation at 314 nm, is plotted as a function of temperature in 0 M NaCl (black triangles), 100 mM NaCl (blue circles), 200 mM NaCl (green circles), and 500 mM NaCl (red circles). (b) The fraction unfolded, obtained from a two-state analysis of the fluorescence emission intensity data in panel a, are plotted as a function of temperature for the three different salt conditions. The symbols are as described for panel a. All measurements were made with ~5 μM strand concentration in 5 mM sodium cacodylate pH 7.0, 50 μM EDTA, and varying NaCl concentrations.

buffer conditions as the Libchaber group[33,34] for our measurements on LS5T21, and as the Van Orden group[32,38] for our measurements on VS4T21. The discrepancy in the thermodynamics of both 4-bp and 5-bp stem, T_{21} loop, hairpins between our measurements and these earlier measurements on rhodamine/dabcyl labeled hairpins is not immediately apparent. Our best guess is that the rhodamine/dabcyl pair tends to add stability to the hairpin stem, perhaps from unforeseen stacking interactions.

Kinetics Measurements from Laser T-Jump. Representative relaxation kinetics traces obtained from the fluorescence measurements in response to a laser T-jump are shown for FRET-labeled VS4T21 (Figure 3) and 2AP labeled LS5T21 (Figure 4) at each of the salt concentrations. The data are well described in terms of a single-exponential relaxation. T-jump measurements on control samples (fluorescein-only strand of DNA or free 2AP) showed no relaxation on these time scales. We also carried out maximum entropy analysis on each of the relaxation traces to detect deviations from single-exponential behavior. All relaxation traces were well described by a distribution of relaxation times with a single dominant peak, as illustrated in Figure S7a (Supporting Information).

The relaxation times at each temperature, obtained from the T-jump measurements, together with the equilibrium constants, obtained from the melting profiles, were analyzed in terms of an apparent two-state system to obtain the folding and unfolding times as a function of temperature (Figures 5 and 6). An Arrhenius fit to the folding/unfolding times yields activation energy parameters that are summarized in Table 2; the folding times exhibit weak temperature dependence with small or negative activation enthalpies, while the unfolding times exhibit much stronger temperature dependence com-
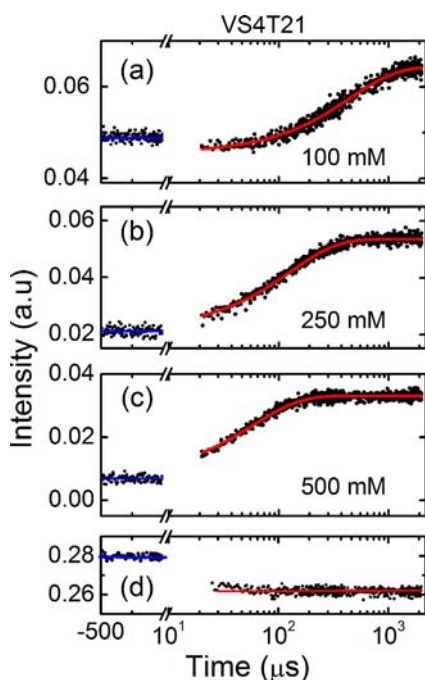
Figure 3. Relaxation kinetics traces for VS4T21 hairpins from T-jump measurements. The fluorescence intensity of double-labeled VS4T21 samples measured at 536 ± 20 nm, with excitation at 488 nm, is plotted as a function of time in response to a T-jump perturbation. The relaxation kinetics shown are in (a) 100 mM NaCl, after a T-jump from 7 to 13 °C, (b) 250 mM NaCl, after a T-jump from 17 to 23 °C, and (c) 500 mM NaCl, after a T-jump from 22 to 25 °C. Measurements were made with strand concentrations (a) 10, (b) 10, and (c) 11 μM. The buffer conditions were as described for Figure 1. (d) The fluorescence intensity of fluorescein-labeled ssDNA strand is plotted as a function of time in response to a T-jump from 24 to 32 °C. The initial drop in intensity is from a change in quantum yield of fluorescein as a result of the T-jump. The subsequent trace shows no relaxation kinetics up to about 2 ms. The continuous red lines in panels a−c are single exponential fits to the relaxation kinetics, with relaxation times 442, 127, and 58 μs, respectively. In panel d the red line represents the average intensity after the T-jump. The blue lines in each of the panels represent the average intensity measured prior to the T-jump perturbation.

Figure 4. Relaxation kinetics traces for LS5T21 hairpins from T-jump measurements. The fluorescence intensity of 2AP-labeled LS5T21 samples measured at 370 ± 18 nm, with excitation at 284 nm, is plotted as a function of time in response to a T-jump perturbation. The relaxation kinetics shown are in (a) 100 mM NaCl, after a T-jump from 17 to 22 °C, (b) 200 mM NaCl, after a T-jump from 16 to 25 °C, and (c) 500 mM NaCl, after a T-jump from 13 to 16 °C. Measurements were made with strand concentrations (a) 25, (b) 50, and (c) 35 μM. The buffer conditions were as described for Figure 2. (d) The fluorescence intensity of free 2AP is plotted as a function of time in response to a T-jump from 13 to 16 °C. The initial drop in intensity is from a change in quantum yield of 2AP as a result of the T-jump. The subsequent trace shows no relaxation kinetics up to about 800 μs. The continuous red lines in panels a−c are single exponential fits to the relaxation kinetics, with relaxation times 80, 60, and 40 μs, respectively. In panel d the red line represents the average intensity after the T-jump. The blue lines in each of the panels represent the average intensity measured prior to the T-jump perturbation.

mensurate with the enthalpy cost of breaking nearly all base pairs in the stem.

Kinetics Measurements from Rapid Mixing. We also investigated the hairpin folding kinetics starting from an unfolded ensemble, under conditions of 0 M NaCl, and using the microfluidic mixing apparatus to rapidly increase NaCl concentration, to initiate the folding. For both hairpins, the equilibrium fluorescence measurements showed no transition at 0 M NaCl, indicating an undetectable population of folded structures prior to the mixing event. Representative relaxation kinetics traces obtained in the rapid mixing apparatus are shown for FRET-labeled VS4T21 (Figure 7) and 2AP-labeled LS5T21 (Figure 8), together with control measurements on the FRET-labeled polythymine (T_{20}) strand and on free 2AP, respectively. For the FRET-labeled hairpin, there is a rapid increase in the proximity ratio (defined in the Experimental Section) within the ∼8 μs mixing time of the apparatus. This increase is observed for both the hairpin and the T_{20} strand, and is attributed to a rapid collapse of the polynucleotide chain as the monovalent ions diffuse into the central jet of the mixing device. Subsequent relaxation kinetics are observed on the time
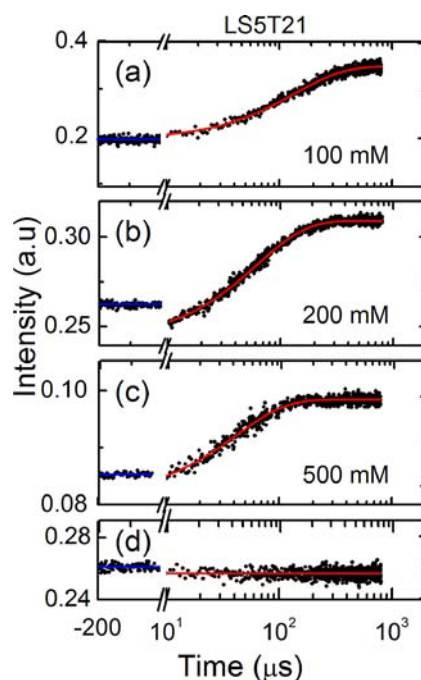
window of ∼10 μs−1 ms for the hairpin but not for the T_{20} strand.

The hairpin relaxation traces are well described in terms of a single-exponential relaxation at all temperatures and salt concentrations measured, with the exception of proximity ratio traces on FRET-labeled VS4T21 in 100 mM NaCl, for which an additional fast phase is observed, although the slower phase has the dominant (60−70%) amplitude. Maximum entropy analysis of relaxation traces obtained in rapid mixing measurements also reveals a predominantly single peak in the distribution of relaxation times, consistent with single-exponential decay, with the exception of data on VS4T21 hairpin in 100 mM NaCl, for which additional peaks are discerned in the distribution (Figure S7b−d, Supporting Information). There may well be a missing fast phase, occurring on time scales faster than ∼10 μs, even at the higher salt conditions, as indicated by the amplitude of the change in the proximity ratio within the dead time of the instrument, which is observed to be about 2 times bigger for the VS4T21 hairpin in 500 mM NaCl than that observed for the polythymine strand (Figure 7).
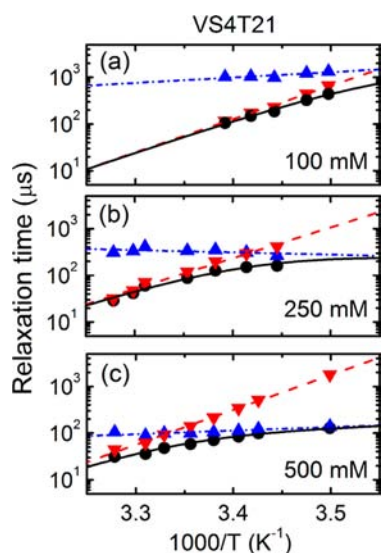
Figure 5. Temperature dependence of relaxation times for VS4T21 hairpins. Relaxation times (black circles) obtained from single-exponential fits to the kinetics traces are plotted as a function of inverse temperature, together with folding (blue triangles) and unfolding (red inverted triangles) times, obtained from a two-state fit to the relaxation kinetics, for VS4T21 hairpins in (a) 100, (b) 250, and (c) 500 mM NaCl. The continuous lines are the best fit to the temperature dependence of the relaxation times assuming Arrhenius dependence for the folding (blue dashed-dot lines) and unfolding (red dashed lines) times. The best fit parameters are summarized in Table 2.
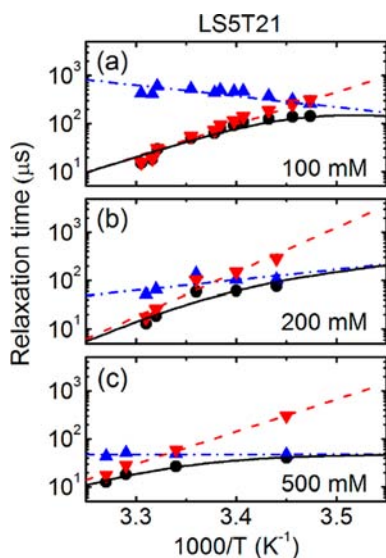

Figure 6. Temperature dependence of relaxation times for LS5T21 hairpins. Relaxation times (black circles) obtained from single-exponential fits to the kinetics traces are plotted as a function of inverse temperature, together with folding (blue triangles) and unfolding (red inverted triangles) times, obtained from a two-state fit to the relaxation kinetics, for LS5T21 hairpins in (a) 100, (b) 200, and (c) 500 mM NaCl. The continuous lines are the best fit to the temperature dependence of the relaxation times assuming Arrhenius dependence for the folding (blue dashed-dot lines) and unfolding (red dashed lines) times. The best fit parameters are summarized in Table 2.

To examine any evidence for significant missing amplitudes at long times, we compared the relative contributions of the

Table 2. Folding/Unfolding Times from Two-State Analysis of Relaxation Rates in T-Jump Measurements and Corresponding Activation Enthalpies from Arrhenius Fits

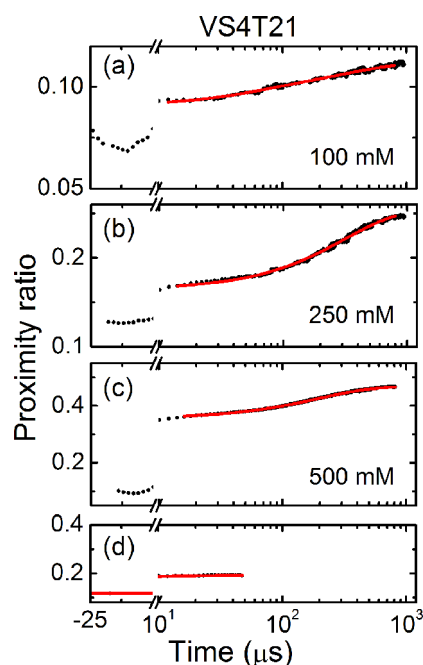|	VS4T21	VS4T21	VS4T21	LS5T21	LS5T21	LS5T21
[NaCl] (mM)	100	250	500	100	200	500
τ_F at 25 °C (μs)	988	311	113	381	101	48
$\Delta H^{\ddagger}_F$ (kcal/mol)	5.3	−2.3	3.4	−5.8	2.4	0.1
τ_U at 25 °C (μs)	128	233	315	89	135	132
$\Delta H^{\ddagger}_U$ (kcal/mol)	32.8	30.3	34.4	35.5	34.9	30.9

Figure 7. Relaxation kinetics traces for VS4T21 hairpin from rapid mixing measurements. Proximity ratio traces, measured on double-labeled VS4T21 hairpins initially in 0 M NaCl, are plotted as a function of time (black circles) after mixing into final salt conditions of (a) 100 mM NaCl at 9 °C, (b) 250 mM NaCl at 15 °C, and (c) 500 mM NaCl at 20 °C. The red lines are single-exponential fits through the data points, with characteristic relaxation times of (a) 1.2 ms, (b) 359 μs, and (c) 207 μs. All measurements were made with 720 nM strand concentrations. The buffer conditions were as described for Figure 1. (d) Proximity ratio traces, measured on double-labeled polythymine T$_{20}$ after the addition of 500 mM NaCl at 23 °C, are plotted as a function of time. The initial increase in the signal corresponds to the collapse of the polymer upon rapid increase in the salt concentration. No subsequent relaxation is observed after about 10 μs. The red line is the computed concentration of salt versus time before and after mixing.

donor and acceptor fluorescence to the emission spectra of FRET-labeled hairpins at the end of the rapid mixing time window (~1 ms after mixing) and that obtained under equilibrium conditions, as shown in Figure S8 (Supporting Information). The two spectra agree remarkably well at high (500 mM) NaCl concentration (Figure S8c), indicating no significant missing amplitude beyond ~1 ms at these ionic conditions. The relaxations in 100 and 250 mM NaCl are not fully completed on this time window, as is evident from the spectral comparison (Figure S8a,b), and the ~1 ms relaxation
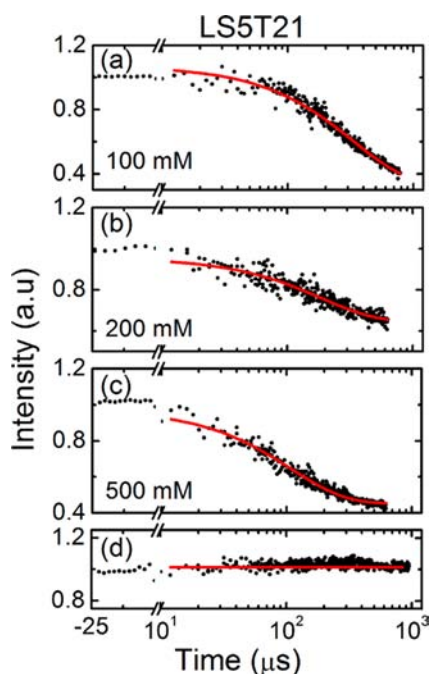
Figure 8. Relaxation kinetics traces for LS5T21 hairpin from rapid mixing measurements. Fluorescence emission intensity traces, measured on 2AP-labeled LS5T21 hairpins initially in 0 M NaCl, are plotted as a function of time (black circles) after mixing into final salt conditions of (a) 100 mM NaCl at 10 °C, (b) 200 mM NaCl at 23 °C, and (c) 500 mM NaCl at 23 °C. The red lines are single-exponential fits through the data points, with characteristic relaxation times of (a) 310, (b) 338, and (c) 100 μs. All measurements were made with 100 μM strand concentrations. The buffer conditions were as described for Figure 2. (d) Fluorescence emission intensity traces, measured on free 2AP under identical mixing conditions as in panel c, are plotted as a function of time. No relaxation kinetics are observed.

times obtained for the dominant component in the rapid mixing measurements, at the two lower salt conditions. Missing amplitude analysis was not carried out for the 2AP-labeled hairpins because of the difficulty in absolute comparison of transient and equilibrium spectra.

Comparison of Relaxation Times from T-Jump and Rapid Mixing Measurements. The predominantly single-exponential behavior observed for all relaxation traces measured in the T-jump and rapid mixing time and temperature window is suggestive of a two-state system, although single-exponential kinetics are by no means a sufficient condition for two-state behavior; downhill folding scenarios can also yield single-exponential relaxation kinetics, as observed in some protein-folding studies.[45−49] One test of two-state behavior is whether the two distinct perturbation techniques, T-jump and rapid mixing, will yield identical relaxation kinetics. In Figures 9 and 10, we compare the relaxation times obtained from these two techniques for each of the hairpins at the three different salt conditions. The results are quite striking in that the relaxation times obtained from the rapid mixing measurements, although similar to the relaxation times obtained from the T-jump measurements at low temperatures, tend to be slower as the temperature is raised, and approach greater than 10-fold discrepancy at temperatures near 30 °C, which is in the vicinity of, or higher than, the T_m of all the hairpins/ionic conditions in this study. To rule out any discrepancy due to the different probes used for the FRET-labeled samples in T-jump (donor
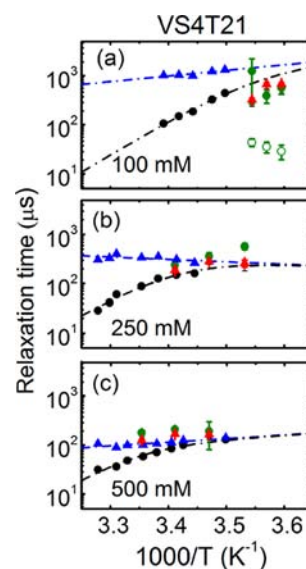

Figure 9. Comparison of relaxation times from T-jump and rapid mixing measurements for VS4T21 hairpins. Relaxation times obtained from T-jump (black circles) and rapid mixing (green circles from proximity ratio analysis and red triangles from donor intensity analysis) are plotted versus inverse temperature in (a) 100, (b) 250, and (c) 500 mM NaCl. In panel a, the rapid mixing measurements from the proximity ratio analysis are better described in terms of two exponentials, with a fast component (green open circles) and a slow component (green filled circles). The folding times, obtained from an apparent two-state analysis of the T-jump kinetics and equilibrium thermodynamics, are included in each of the panels (blue triangles).
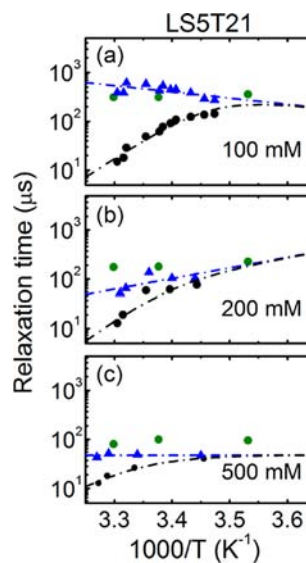

Figure 10. Comparison of relaxation times from T-jump and rapid mixing measurements for LS5T21 hairpins. Relaxation times obtained from T-jump (black circles) and rapid mixing (green circles) are plotted versus inverse temperature in (a) 100, (b) 200, and (c) 500 mM NaCl, together with the folding times obtained from the T-jump measurements (blue triangles), as described for Figure 9.

intensity) and rapid mixing (proximity ratio), we also analyzed the relaxation traces obtained from the donor intensity channel only in the rapid mixing measurements. The two probes yield consistent results for the rapid mixing data, as shown in Figure 9, although the donor intensity analysis did not yield the fast

component seen by the proximity ratio analysis in 100 mM NaCl.

The distinct relaxation times obtained from the two different perturbation techniques on both hairpins rule out a two-state approximation for nucleic acid hairpin folding/unfolding kinetics at a coarse-grained level, even at temperatures near T_m, and suggest that the unfolded ensemble accessed after the initial collapse of the chain, induced by the addition of counterions, is distinctly different from the unfolded ensemble as a result of the T-jump perturbation.

An unexpected result from these studies is that the *folding* times extracted from an apparent two-state approximation of the T-jump kinetics are in reasonably good agreement with the *relaxation* times obtained from the ion-jump experiments, over the entire range of temperature and ionic conditions that were explored, as shown in Figures 9 and 10. Although this comparison is inherently problematic, since even in the ion-jump measurements the relaxation times must include contributions from both folding and unfolding times, the close agreement between the T-jump folding times and the rapid mixing relaxation times suggests that the latter predominantly measures the escape from the collapsed ensemble, even at temperatures above T_m. This interpretation then indicates that the collapsed ensemble is a transient in the ion-jump measurements that is not accessible with any significant probability in the T-jump measurements.

◼ DISCUSSION

Free energy landscape theory has provided a useful framework for understanding folding pathways for biological macromolecules,[50−52] but there have been few direct tests of the multidimensional aspect of the theory. This is primarily due to either the limited number of spectroscopic probes or the limited time window of measurements. By combining methods that potentially explore different regions of the folding landscape we can better characterize it, particularly at the top of the folding funnel where conformational space is larger.

This study was partially motivated by FCS measurements on labeled DNA hairpins by the Van Orden group which yielded indirect evidence for a three-state folding mechanism for DNA hairpins with large (T_{21}) loops, with stable intermediates in the folding pathway, possibly from collapsed states, that were postulated to linger on time scales of hundreds of microseconds before folding to the native state in a second relaxation occurring on time scales much slower than milliseconds. Although deviations from single exponential kinetics in the folding of ssDNA and RNA hairpins have been observed in laser T-jump measurements at temperatures far above or below the melting temperatures T_m of the hairpins,[21,22,24,31] these relaxation kinetics have all been observed on submillisecond time scales, leaving open the possibility that T-jump and FCS measurements may be exploring different regions of the folding energy landscape.

In this study we have investigated the multidimensionality of the landscape of nucleic acid hairpin formation with two different methods of initiating folding/unfolding. The first method is laser temperature-jump, which rapidly raises the temperature of the sample by several degrees and destabilizes the folded hairpin conformation; the second method is rapid mixing with counterions, which stabilizes the folded hairpin. The relaxation kinetics are monitored by either FRET, which measures the distance between the two ends of the hairpin, or

2-aminopurine fluorescence, which measures the local environment of the nucleotide analogue placed in the hairpin stem.

The two probes of the conformational ensemble reveal qualitatively similar thermodynamics and kinetics, with predominantly single-exponential relaxation traces observed in both T-jump and rapid mixing time windows, over the temperature and ionic conditions studied, as illustrated by a single peak in the distribution of relaxation times needed to describe the kinetics traces (Figure S7a, Supporting Information). The one exception is proximity ratio measurements on the FRET-labeled VS4T21 hairpin in the rapid mixing apparatus, where we observe two relaxation phases in 100 mM NaCl, with characteristic relaxation times of 30−45 μs, and 400 μs-1.2 ms, measured in the temperature range 5−9 °C. Biphasic kinetics on similar time scales, with relaxation times of 84 and 393 μs, were also observed in FCS measurements on a hairpin with identical sequence and under identical buffer/salt conditions at 20 °C,[38] and predicted in coarse-grained simulations of folding kinetics of small RNA hairpins.[12] At higher salt concentrations of 250 and 500 mM NaCl, or when the rapid mixing kinetics are analyzed by using donor intensity (in VS4T21) or 2AP fluorescence (in LS5T21) as a probe, the fast component has either negligible amplitude or is too fast to be resolved on the rapid mixing time scales.

The observed relaxation kinetics are predominantly on submillisecond time scales, with little or no evidence for any significant residual population at times longer than the T-jump or rapid mixing time window. This result is evident for the FRET-labeled VS4T21 hairpins at high (500 mM) NaCl, as indicated by a comparison of the shape of their emission spectra obtained at the end of the rapid mixing relaxation traces, and that obtained under equilibrium conditions (Figure S8, Supporting Information). Although a similar analysis could not be carried out on the 2AP-labeled LS5T21 hairpin measurements because of the inherent difficulty in comparing absolute intensities of spectra measured under transient and equilibrium conditions, a recent stopped-flow study, carried out by the Van Orden group on their 5-bp stem, T_{21} loop hairpin (with sequence very similar to our LS5T21), also showed that, in 500 mM NaCl, the relaxation was complete within the dead time of the stopped-flow measurements.[53] In 100 mM NaCl, the stopped-flow measurements yielded relaxation time of ~0.8 ms, which is within a factor of 3 of our value of ~0.3 ms for LS5T21 and 1.2 ms for the VS4T21, obtained in the rapid mixing measurements, indicating that we are at most missing the tail end of the observed relaxation traces even at low salt. However, these results are in apparent contradiction with the earlier FCS study from the Van Orden group that postulated a long-lived (metastable) intermediate state for their 5-bp stem, T_{21} loop hairpin, with the amplitude of the (missing) slow relaxation predicted to increase at 500 mM NaCl.[32] Whether these discrepancies are the result of slight variations in the stem sequences, or variations in labeling strategies that perhaps account for the very different stabilities of similar hairpins in different studies, or due to distinct regions of the energy landscape sampled in the various experimental techniques, remains unclear.

The more interesting result from this study is that the relaxation kinetics initiated from different initial conditions (T-jump or ion-jump) are distinctly different, despite the identical probes and identical final buffer/salt conditions in the two sets of measurements. For both hairpins and at all ionic conditions studied, the slower (or sole) component from rapid mixing is

comparable to T-jump relaxation times in the vicinity of ~10 °C, but deviates and gets slower than T-jump values as the temperature is raised to ~30 °C. As an example, for the LS5T21 hairpin at 20 °C and 100 mM NaCl (final temperature and ionic condition), we measure a relaxation time of 128 μs in T-jump and 314 μs in rapid mixing. At 30 °C, T-jump yields relaxation times in the range of 12−32 μs for all three ionic conditions, while rapid mixing yields 310, 175, and 80 μs, at 100, 200, and 500 mM NaCl, respectively. Thus, at high temperatures, the difference in the relaxation times obtained from the two techniques exceeds 10-fold. This result is contrary to what is expected if the folded and unfolded ensembles are distinct valleys separated by a significant free energy barrier, since in this case the initial populations in the two valleys prior to the perturbation should not affect the measured relaxation times. Our results clearly show that such a simplified two-state approximation breaks down, and indicate that the unfolded ensembles in T-jump and rapid mixing occupy different regions of the energy landscape and follow distinct folding pathways. Similar discrepancies between T-jump and rapid mixing studies have been observed in the folding/unfolding kinetics of a 35-residue subdomain of the villin headpiece protein, with folding initiated by rapid dilution of denaturant occurring 4−5 times slower than relaxation kinetics in response to T-jump perturbation.[54]

To understand this phenomenon, we recognize that in the absence of counterions, the single-stranded polymer is in a highly extended state due to increased electrostatic repulsion in the charged polymer, as is evident from our static FRET (acceptor ratio) measurements. These results are consistent with recent persistence length measurements on unstructured ssDNA and RNA strands, carried out by Pollack, Webb, and co-workers, which showed a significant drop in the persistence length measured for both poly(dT) and poly(rU) strands with increasing salt concentration, with values for dT_{40} decreasing from 2.1 nm in 0 M NaCl to 1.65 nm in 100 mM NaCl and 1.05 nm in 1 M NaCl.[55]

It is important to keep in mind that, although the initial, unfolded state in zero salt (prior to mixing) is highly extended, rapid mixing with counterions results in a collapse of the chain within the ~8 μs mixing time. This initial collapse is observed in the FRET measurements on both VS4T21 as well as the polythymine chain. Notably, the initial increase in proximity ratio (or decrease in the end-to-end distance) within the mixing time is larger in amplitude for the hairpin than for the polythymine chain (Figure 7). These data indicate additional compaction in the hairpin strand, plausibly from native and non-native Watson−Crick (WC) and non-WC hydrophobic/stacking interactions, over and above the collapse of the polymer triggered by charge neutralization. The rapid phase observed after ion-jump to 100 mM NaCl conditions may well be the tail end of this additional compaction kinetics, with the slow phase corresponding to conformational rearrangements in the collapsed state to form the folded hairpin.[8,56]

A glimpse of different folding pathways starting from different initial conditions for RNA hairpins in a multidimensional landscape has already come from coarse-grained simulation studies of Thirumalai and co-workers,[10,12] with folding initiated from an initially thermally unfolded ensemble (by temperature-quench, a rapid decrease in temperature) or from an initially mechanically stretched state (by force-quench, or removal of the stretching force), and more recently for an RNA pseudoknot,[57] with folding initiated by temperature-

quench or ion-jump. The RNA hairpin simulations show nearly 10-fold slower refolding times in force-quench in comparison with temperature-quench,[10] similar to the experimental discrepancies between rapid mixing and T-jump reported here. This comparison suggests that the initial unfolded state in the absence of counterions (prior to mixing) may be similar to the mechanically stretched state, with similar folding trajectories that sample a much larger conformational space prior to folding in comparison with conformational space sampled in T-jump. Figure 11 illustrates this concept. The
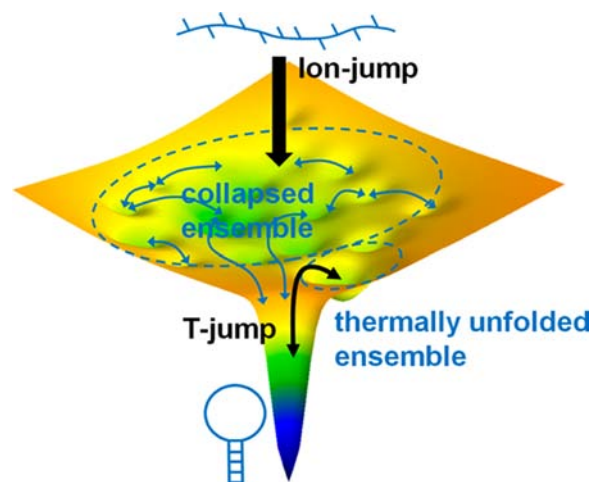

Figure 11. Free energy landscape for nucleic acid hairpins. A schematic of the free energy landscape illustrates at least two distinct regions in the unfolded ensemble corresponding to the collapsed state accessed after ion-jump, and the thermally unfolded state accessed after T-jump. Configurational diffusion in the unfolded region between misfolded microstates is represented by the blue arrows.

unfolded basin is very broad and has many local minima (i.e., roughness). The mixing experiment, in which the highly extended chain collapses during mixing, occupies a larger region of this landscape than the T-jump experiment because the latter perturbs the unfolded ensemble far less.

The folding kinetics initiated by the rapid ion-jump are nearly independent of temperature, with the relaxation rate increasing as the folding bias increases, at higher (final) ion concentrations. In contrast, relaxation rates for kinetics initiated by T-jump at a fixed ion concentration increase with increasing temperature. In a two-state approximation of the thermodynamics (from thermal melting profiles) and relaxation kinetics from T-jump, the observed temperature dependence is as anticipated, with relaxation rates at temperatures above T_m dominated by the unfolding rate, as the free energy bias tilts toward the thermally unfolded ensemble. An intriguing observation from our studies is that the *folding* times thus extracted from T-jump measurements are in surprising agreement with the *relaxation* times obtained from the ion-jump measurements, over the entire range of final temperature and ionic conditions. One explanation for this behavior is that the unfolded (collapsed) ensemble accessed by the ion-jump in the mixer is comprised of misfolded conformations that are higher in free energy than the folded or unfolded states accessed by rapidly increasing the temperature. In this case, the relaxation times obtained in the ion-jump measurements will be dominated by the rate of escape from the collapsed ensemble even at temperatures above the T_m of the hairpin, followed by

rapid reequilibration among microstates of the system accessible by T-jump.

A recent Markov State Model by Pande and co-workers of an 8-nucleotide RNA hairpin found multiple non-native states each directly connected to the native state, with transitions between these non-native states slower than transitions to the folded state.[15] Should some of these non-native states represent the collapsed ensemble accessed in mixing experiments and others represent the thermally unfolded ensemble accessed in the T-jump experiment, the observed kinetics could represent the set of pathways selected by each technique. Finally, we cannot rule out that the dominant contribution to the relaxation/folding times measured by ion-jump/T-jump is from diffusive search on a relatively flat energy landscape, as was invoked in a recent statistical mechanical description of the hairpin dynamics that successfully captured the thermodynamics and temperature/loop-size dependence of their folding/unfolding kinetics.[56]

CONCLUSION

We have combined ion-jump in microfluidic mixing and temperature-jump experiments to explore the multidimensionality of the free energy landscape accessible to a nucleic acid hairpin. Although both sets of measurements indicate predominantly single-exponential relaxation kinetics that are essentially complete on the microsecond-to-submillisecond time window accessible to both techniques, the relaxation times obtained from the two very different perturbation methods are quite distinct, especially at temperatures above the T_m of the hairpins. These measurements rule out a simple two-state description of the folding/unfolding kinetics and reveal a rather rugged folding energy landscape, with implications of configurational diffusion on a broad, relatively flat energy landscape characterizing the dynamics in the unfolded ensemble, but one with distinct folding/refolding pathways starting from different regions in the energy landscape, as a result of the different perturbations. Further progress in elucidating the nature of the microstates accessible in each of the perturbation techniques will come from a more thorough thermodynamic description of the folding/unfolding phase diagram, as a function of both temperature and ionic conditions, as was done in a recent simulations study of RNA pseudoknots,[57] and by potentially extending the time resolution of ion-jump measurements to access the kinetics of the initial collapse transition.

ASSOCIATED CONTENT

Ⓢ Supporting Information

Description of differential scanning calorimetry measurements; description of maximum entropy analysis to obtain distribution of relaxation times; contour plots of fluorescence within the microfluidic mixer (Figure S1); fluorescence emission spectra of FRET-labeled VS4T21 (Figure S2); absorbance melting measurements on unlabeled VS4T21 (Figure S3); fluorescence emission spectra of 2AP-labeled LS5T21 (Figure S4); absorbance melting measurements on unlabeled LS5T21 (Figure S5); differential scanning calorimetry measurements on unlabeled hairpins (Figure S6); maximum entropy analysis of relaxation traces (Figure S7); and comparison of fluorescence emission spectra from kinetics and equilibrium measurements (Figure S8). This material is available free of charge via the Internet at http://pubs.acs.org.

AUTHOR INFORMATION

Corresponding Author
ansari@uic.edu; lapidus@msu.edu

Present Address
‡School of Physical and Mathematical Sciences, Division of Chemistry & Biological Chemistry, Nanyang Technological University, Singapore

Author Contributions
±R.N. and L.Z. contributed equally to this work.

Notes
The authors declare no competing financial interest.

REFERENCES

(1) Dai, X.; Greizerstein, M. B.; Nadas-Chinni, K.; Rothman-Denes, L. B. *Proc. Natl. Acad. Sci. U.S.A.* **1997**, *94*, 2174−2179.
(2) Dai, X.; Kloster, M.; Rothman-Denes, L. B. *J. Mol. Biol.* **1998**, *283*, 43−58.
(3) Glucksmann-Kuis, M. A.; Dai, X.; Markiewicz, P.; Rothman-Denes, L. B. *Cell* **1996**, *84*, 147−154.
(4) Roth, D. B.; Menetski, J. P.; Nakajima, P. B.; Bosma, M. J.; Gellert, M. *Cell* **1992**, *70*, 983−991.
(5) Kennedy, A. K.; Guhathakurta, A.; Kleckner, N.; Haniford, D. B. *Cell* **1998**, *95*, 125−134.
(6) Bevilacqua, P. C.; Blose, J. M. *Annu. Rev. Phys. Chem.* **2008**, *59*, 79−103.
(7) Woodson, S. A. *Annu. Rev. Biophys.* **2010**, *39*, 61−77.
(8) Sorin, E. J.; Rhee, Y. M.; Nakatani, B. J.; Pande, V. S. *Biophys. J.* **2003**, *85*, 790−803.
(9) Nivon, L. G.; Shakhnovich, E. I. *J. Mol. Biol.* **2004**, *344*, 29−45.
(10) Hyeon, C.; Thirumalai, D. *Proc. Natl. Acad. Sci. U.S.A.* **2005**, *102*, 6789−6794.
(11) Kannan, S.; Zacharias, M. *Biophys. J.* **2007**, *93*, 3218−3228.
(12) Hyeon, C.; Thirumalai, D. *J. Am. Chem. Soc.* **2008**, *130*, 1538−1539.
(13) Bowman, G. R.; Huang, X.; Yao, Y.; Sun, J.; Carlsson, G.; Guibas, L. J.; Pande, V. S. *J. Am. Chem. Soc.* **2008**, *130*, 9676−9678.
(14) Garcia, A. E.; Paschek, D. *J. Am. Chem. Soc.* **2008**, *130*, 815−817.
(15) Huang, X.; Yao, Y.; Bowman, G. R.; Sun, J.; Guibas, L. J.; Carlsson, G.; Pande, V. S. *Pac. Symp. Biocomput.* **2010**, *15*, 228−239.
(16) Deng, N. J.; Cieplak, P. *Biophys. J.* **2010**, *98*, 627−636.
(17) Cantor, C. R.; Schimmel, P. R. *Biophysical Chemistry Part III: The Behavior of Biological Macromolecules*; W. H. Freeman and Company: New York, 1980.
(18) Coutts, S. M. *Biochim. Biophys. Acta* **1971**, *232*, 94−106.
(19) Gralla, J.; Crothers, D. M. *J. Mol. Biol.* **1973**, *73*, 497−511.
(20) Porschke, D. *Biophys. Chem.* **1974**, *1*, 381−386.
(21) Ma, H.; Proctor, D. J.; Kierzek, E.; Kierzek, R.; Bevilacqua, P. C.; Gruebele, M. *J. Am. Chem. Soc.* **2006**, *128*, 1523−1530.
(22) Stancik, A. L.; Brauns, E. B. *Biochemistry* **2008**, *47*, 10834−10840.
(23) Sarkar, K.; Nguyen, D. A.; Gruebele, M. *RNA* **2010**, *16*, 2427−2434.
(24) Ma, H.; Wan, C.; Wu, A.; Zewail, A. H. *Proc. Natl. Acad. Sci. U.S.A.* **2007**, *104*, 712−716.
(25) Ansari, A.; Kuznetsov, S. V. *J. Phys. Chem. B* **2005**, *109*, 12982−12989.

(26) Narayanan, R.; Velmurugu, Y.; Kuznetsov, S. V.; Ansari, A. *J. Am. Chem. Soc.* **2011**, *133*, 18767−18774.

(27) Kuznetsov, S. V.; Ren, C.; Woodson, S. A.; Ansari, A. *Nucleic Acids Res.* **2008**, *36*, 1098−1112.

(28) Porschke, D. *Biophys. Chem.* **1974**, *2*, 97−101.

(29) Porschke, D. *Biophys. Chem.* **1974**, *2*, 83−96.

(30) Ansari, A.; Kuznetsov, S. V.; Shen, Y. *Proc. Natl. Acad. Sci. U.S.A.* **2001**, *98*, 7771−7776.

(31) Sarkar, K.; Meister, K.; Sethi, A.; Gruebele, M. *Biophys. J.* **2009**, *97*, 1418−1427.

(32) Jung, J.; Van Orden, A. *J. Am. Chem. Soc.* **2006**, *128*, 1240−1249.

(33) Bonnet, G.; Krichevsky, O.; Libchaber, A. *Proc. Natl. Acad. Sci. U.S.A.* **1998**, *95*, 8602−8606.

(34) Goddard, N. L.; Bonnet, G.; Krichevsky, O.; Libchaber, A. *Phys. Rev. Lett.* **2000**, *85*, 2400−2403.

(35) Wallace, M. I.; Ying, L.; Balasubramanian, S.; Klenerman, D. *Proc. Natl. Acad. Sci. U.S.A.* **2001**, *98*, 5584−5589.

(36) Gurunathan, K.; Levitus, M. *J. Phys. Chem. B* **2010**, *114*, 980−986.

(37) Kim, J.; Doose, S.; Neuweiler, H.; Sauer, M. *Nucleic Acids Res.* **2006**, *34*, 2516−2527.

(38) Jung, J.; Ihly, R.; Scott, E.; Yu, M.; Van Orden, A. *J. Phys. Chem. B* **2008**, *112*, 127−133.

(39) Clegg, R. M. *Methods Enzymol.* **1992**, *211*, 353−388.

(40) Knight, J. B.; Vishwanath, A.; Brody, J. P.; Austin, R. H. *Phys. Rev. Lett.* **1998**, *80*, 3863−3866.

(41) Hertzog, D. E.; Michalet, X.; Jager, M.; Kong, X.; Santiago, J. G.; Weiss, S.; Bakajin, O. *Anal. Chem.* **2004**, *76*, 7169−7178.

(42) Hertzog, D. E.; Ivorra, B.; Mohammadi, B.; Bakajin, O.; Santiago, J. G. *Anal. Chem.* **2006**, *78*, 4299−4306.

(43) Yao, S.; Bakajin, O. *Anal. Chem.* **2007**, *79*, 5753−5759.

(44) Waldauer, S. A.; Bakajin, O.; Ball, T.; Chen, Y.; DeCamp, S. J.; Kopka, M.; Jager, M.; Singh, V. R.; Wedemeyer, W. J.; Weiss, S.; Yao, S.; Lapidus, L. J. *HFSP J.* **2008**, *2*, 388−395.

(45) Ma, H.; Gruebele, M. *Proc. Natl. Acad. Sci. U.S.A.* **2005**, *102*, 2283−2287.

(46) Liu, F.; Du, D.; Fuller, A. A.; Davoren, J. E.; Wipf, P.; Kelly, J. W.; Gruebele, M. *Proc. Natl. Acad. Sci. U.S.A.* **2008**, *105*, 2369−2374.

(47) DeCamp, S. J.; Naganathan, A. N.; Waldauer, S. A.; Bakajin, O.; Lapidus, L. J. *Biophys. J.* **2009**, *97*, 1772−1777.

(48) Li, P.; Oliva, F. Y.; Naganathan, A. N.; Munoz, V. *Proc. Natl. Acad. Sci. U.S.A.* **2009**, *106*, 103−108.

(49) Cellmer, T.; Buscaglia, M.; Henry, E. R.; Hofrichter, J.; Eaton, W. A. *Proc. Natl. Acad. Sci. U.S.A.* **2011**, *108*, 6103−6108.

(50) Thirumalai, D.; Woodson, S. A. *Acc. Chem. Res.* **1996**, *29*, 433−439.

(51) Onuchic, J. N.; Luthey-Schulten, Z.; Wolynes, P. G. *Annu. Rev. Phys. Chem.* **1997**, *48*, 545−600.

(52) Weinkam, P.; Zong, C.; Wolynes, P. G. *Proc. Natl. Acad. Sci. U.S.A.* **2005**, *102*, 12401−12406.

(53) Nayak, R. K.; Peersen, O. B.; Hall, K. B.; Van Orden, A. *J. Am. Chem. Soc.* **2012**, *134*, 2453−2456.

(54) Zhu, L.; Ghosh, K.; King, M.; Cellmer, T.; Bakajin, O.; Lapidus, L. J. *J. Phys. Chem. B* **2011**, *115*, 12632−12637.

(55) Chen, H.; Meisburger, S. P.; Pabit, S. A.; Sutton, J. L.; Webb, W. W.; Pollack, L. *Proc. Natl. Acad. Sci. U.S.A.* **2012**, *109*, 799−804.

(56) Kuznetsov, S. V.; Ansari, A. *Biophys. J.* **2012**, *102*, 101−111.

(57) Biyun, S.; Cho, S. S.; Thirumalai, D. *J. Am. Chem. Soc.* **2011**, *133*, 20634−20643.

18963

dx.doi.org/10.1021/ja301218e | *J. Am. Chem. Soc.* 2012, 134, 18952−18963